doi:10.1038/nature10257

Supplementary Methods

Additional characterization of detergent-reconstituted UCP2 sample

Proton translocation assay. Proton translocation activity of UCP2 was measured using a liposome-based assay. To prepare proteoliposomes, total brain lipids extract (Avanti) at 20 mg/ml in Buffer A (10 mM citrate, pH 6.1, 100 mM NaCl) + 0.5% decyl-maltoside (DM) was added to 0.5 mM UCP2 NMR sample at a 400:1 lipid:protein ratio and then diluted 20x to a lipid concentration of 1mg/ml with Buffer A + 10 μM of the florescent pH sensitive probe HPTS (8-Hydroxypyrene-1,3,6-Trisulfonic Acid). Detergent removal was performed twice on a G25 column equilibrated with Buffer A alone. Resulting liposomes contain the florescent probe and were stable at room temperature.

For measuring proton translocation, UCP2 proteoliposomes were diluted 10x with Buffer B (10 mM citrate, pH 6.1, 100 mM KCl). Valinomycin was added to increase the permeability of K^+, establishing a membrane potential driven by the K^+ gradient. Under these conditions other positively charged ions would dissipate this potential if their permeability were increased. The H^+ permeability can be increased by the active form of UCP2 or by protonofores like FCCP (**Supplementary Fig. 2a**). In the absence of fatty acid, UCP2 proteoliposomes only show a modest pH increase upon addition of valinomycin within the timeframe of the experiment (**Supplementary Fig. 2b**). When pre-incubated with 1 mM myristic acid, UCP2 proteoliposmes show a rapid increase of the internal pH upon addition of valinomycin (**Supplementary Fig. 2c**), indicating that proton translocation is activated by the fatty acid. UCP2 proteoliposomes pre-incubated with 0.2 mM myristic acid in the presence of 50 μM GDP show only a modest increase in the internal pH (**Supplementary Fig. 2d**), indicating that GDP inhibits proton translocation. Finally, in the presence of 50 μM GDP, increasing the myristic acid concentration to 1 mM leads to partial recovery of proton conductance (**Supplementary Fig. 2e**).

Electron Microscopy Analysis. UCP2 NMR samples at a concentration of 0.5 mM were diluted 1000 fold into a 10 mM HEPES, 40 mM NaCl buffer at pH 7.4 containing 0.03% dodecylphosphocholine (DPC). The diluted sample was then applied to carbon coated EM grids (EMS), washed 3x with water, stained with uranyl acetate and dried quickly under an air stream. Images were recorded at 120 kV on a FEI Tecnai T12 electron microscope equipped with a 4k x 4k Gatan CCD camera (**Supplementary Fig. 3**).

Preparation of DNA nanotubes and aligned sample

The modified M13-based vector p7308 was generated at the nanomole scale as described previously[1]. Presented here is an updated protocol for folding and purification of the nanotubes. We discovered that ethanol precipitation damages the DNA nanostructures, thus more consistent preparations can be obtained by using PEG precipitation instead. Staple-strand oligodeoxyribonucleotides (described previously) were ordered on the 200 nanomole scale, maximum yield requested (for cost-saving reasons), from Invitrogen in desalted, dried format. The strands, whose yields varied compared to each other, were resuspended and pooled ("front monomer" and "rear monomer" pools as described previously) to an average concentration of 1 micromolar per strand, as indicated by spectrophotometer measurements assuming an extinction coefficient of 33 mg/mL for A260 = 1. Monomers were folded at 120 nM scaffold, 720 nM average each staple strand, 5 mM Tris Cl, 1 mM EDTA, pH 8.0, 20 mM $MgCl_2$, in 96-well plates with 150 µL per well (36 mL each monomer). The folding ramp used was as follows: hold at 80ºC for five minutes, then decrease by one degree C every five minutes to 65ºC, then decrease by one degree C every 40 minutes to 20ºC. Each monomer sample was pooled and applied separately to a Qiagen-Tip 10000 Column pre-equilibrated with 75 mL QBT buffer, washed with six rounds of 100 mL QC Buffer, then eluted with 100 mL QF buffer and titrated to 30 mM $MgCl_2$ by addition of 3 mL of a 1 M $MgCl_2$ solution. Equal volumes of the front and rear monomer were combined and incubated at 37ºC for 2 hours to achieve heterodimerization. The nanotubes then were precipitated by addition of 0.25 volumes of 20% PEG8000 followed by incubation at room temperature for 15 minutes. The nanotubes were recovered by centrifugation at 15000 x g for 30 minutes at 4ºC and resuspended in 2.5 mM Tris, 0.5 mM EDTA, pH 8.0, 10 mM $MgCl_2$. Aggregates were removed by further centrifugation of the suspended material at 15000 x g for 15 minutes at 4ºC. The nanotubes in the supernatant then were concentrated to 30 mg/mL in a Centricon-100 concentrator by centrifugation. The nanotube sample is homogeneous as indicated by negative stain EM image (**Supplementary Fig. 4b**).

To prepare the aligned UCP2 sample, we mixed 260 µl of 20 mg/ml nanotubes and 260 µl of 0.5 mM (^{15}N-, ^{13}C, ^{2}H) labeled UCP2 sample containing 5 mM GDP, 100 mM DPC, 2 mM DMPC, 1 mM cardiolipin, 5 mM BME, 30 mM KPi (pH 6.5), and 80 mM NaCl. The mixture was then concentrated down to 260 µl using a Centricon. The final aligned sample gave ^{2}H quadrupolar splitting of 5.0 Hz (**Supplementary Fig. 4c**).

1 Douglas, S. M., Chou, J. J. & Shih, W. M. DNA-nanotube-induced alignment of membrane proteins for NMR structure determination. *Proc Natl Acad Sci U S A* **104**, 6644-6648 (2007).

2 Laskowski, R. A., MacArthur, M. W., Moss, D. S. & Thornton, J. W. PROCHECK: a program to check the stereochemical quality of protein structures. *J. Appl. Cryst.* **26**, 283-291 (1993).

3 Battiste, J. L. & Wagner, G. Utilization of site-directed spin labeling and high-resolution heteronuclear nuclear magnetic resonance for global fold determination of large proteins with limited nuclear overhauser effect data. *Biochemistry* **39**, 5355-5365 (2000).

4 Wang, Y. & Tajkhorshid, E. Electrostatic funneling of substrate in mitochondrial inner membrane carriers. *Proc Natl Acad Sci U S A* **105**, 9598-9603 (2008).

5 Dehez, F., Pebay-Peyroula, E. & Chipot, C. Binding of ADP in the mitochondrial ADP/ATP carrier is driven by an electrostatic funnel. *J Am Chem Soc* **130**, 12725-12733 (2008).

Supplementary Table 1 NMR and refinement statistics for protein structures

	UCP2
NMR distance and dihedral constraints	
Distance constraints (Å)	
Total PRE	452
< 16	23
7 – 17	9
8 – 18	0
9 – 19	11
10 – 20	12
11 – 21	23
12 – 22	49
13 – 23	19
14 – 100	306
Total dihedral angle restraints	454
ϕ (from fragments)	227
ψ (from fragments)	227
Total RDCs	470
Backbone NH	155
Backbone C'Cα	155
Backbone NC'	160
Structure statistics [a]	
Violations (mean ± s.d.)	
Distance constraints (Å)	0.041 ± 0.004
Dihedral angle constraints (º)	1.600 ± 0.064
RDC constraints (Hz)	1.393 ± 0.026
Deviations from idealized geometry	
Bond lengths (Å)	0.005 ± 0.000
Bond angles (º)	0.891 ± 0.016
Impropers (º)	0.988 ± 0.019
Average pairwise r.m.s. deviation (Å)	
Backbone	1.32
Heavy	1.84
Ramachandran plot statistics (%) [c]	
Most favored	95.4
Additionally allowed	3.2
Generally allowed	1.3
Disallowed	0.2

[a] Statistics are calculated and averaged over an ensemble of the 15 low-energy structures.

[b] The precision of the atomic coordinates is defined as the average rms difference between the 15 final structures and their mean coordinates. Only the well-structured segments labeled in Fig. 2c (bottom panel) were included in the calculation.

[c] As evaluated with the program PROCHECK[2], using the regions in (b) above.

Supplementary Table 2 Assignment of PRE-derived distance restraints [a]

Peak intensity ratio of (- ascorbic acid) to (+ ascorbic acid)	Distance constraints used in XPLOR calculation (Å)
< 0.1	< 16
0.1 – 0.2	7 – 17
0.2 – 0.3	8 – 18
0.3 – 0.4	9 – 19
0.4 – 0.5	10 – 20
0.5 – 0.6	11 – 21
0.6 – 0.7	12 – 22
0.7 – 0.75	13 – 23
> 0.75	14 – 100

[a] Distance assignment was based on a previously published calibration[3].

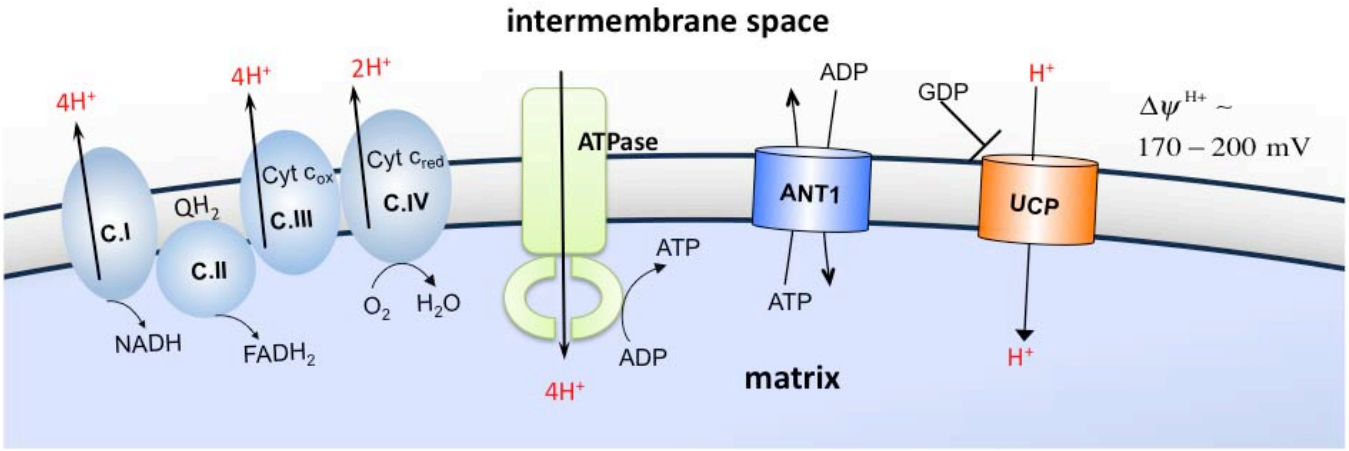

Supplementary Figure 1. Schematic illustration of the physiological role of UCPs in uncoupling respiration from ATP synthesis. Abbreviations are: UCP – uncoupling protein; ANT – adenine nucleotide translocator; C.I – NADH dehydrogenase; C.II – succinate dehydrogenase; C.III – cytochrome bc_1 complex; C.IV – cytochrome *c* oxidase; ATPase – F_OF_1 ATP synthase. GDP inhibits the proton translocation activity of UCP.

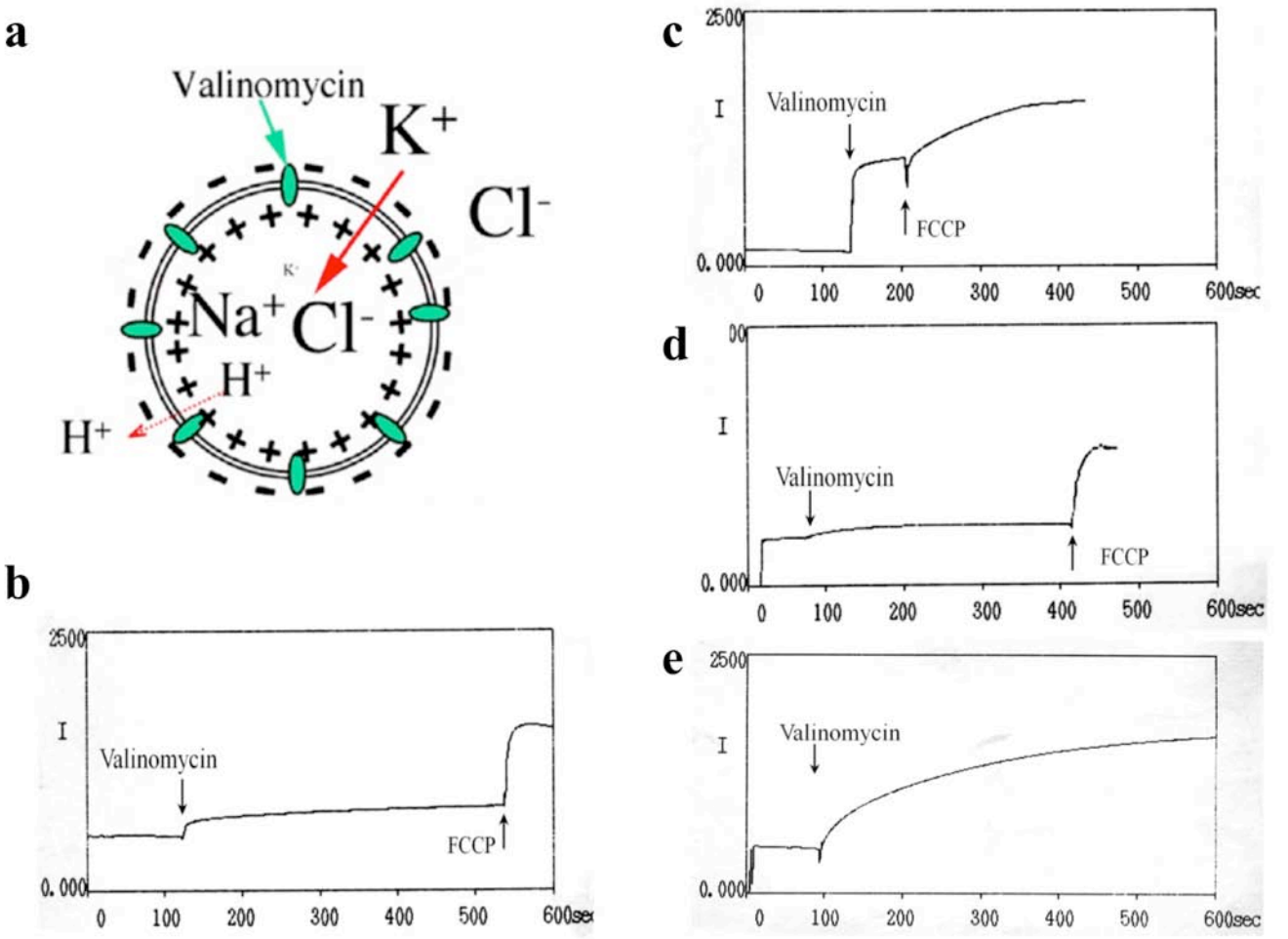

Supplementary Fig. 2. Proton translocation assay of reconstituted UCP2. **a,** Schematic of the liposome assay set up. **b,** UCP2 proteo-liposomes alone show a small proton conductance upon addition of valinomycin. **c,** When 1 mM myristic acid is added in trans, valinomycin elicits a much faster response. **d,** Upon addition of valinomycin, UCP2 proteo-liposomes incubabed with 50 µM GDP and 0.2 mM myristic acid show a proton conductance even smaller than in the case of UCP2 alone (b). **e,** Increasing the myristic acid concentration in (d) to 1 mM partially leads to partial recovery of proton conductance. Towards the end of every experiment, FCCP was added to test vesicle integrity.

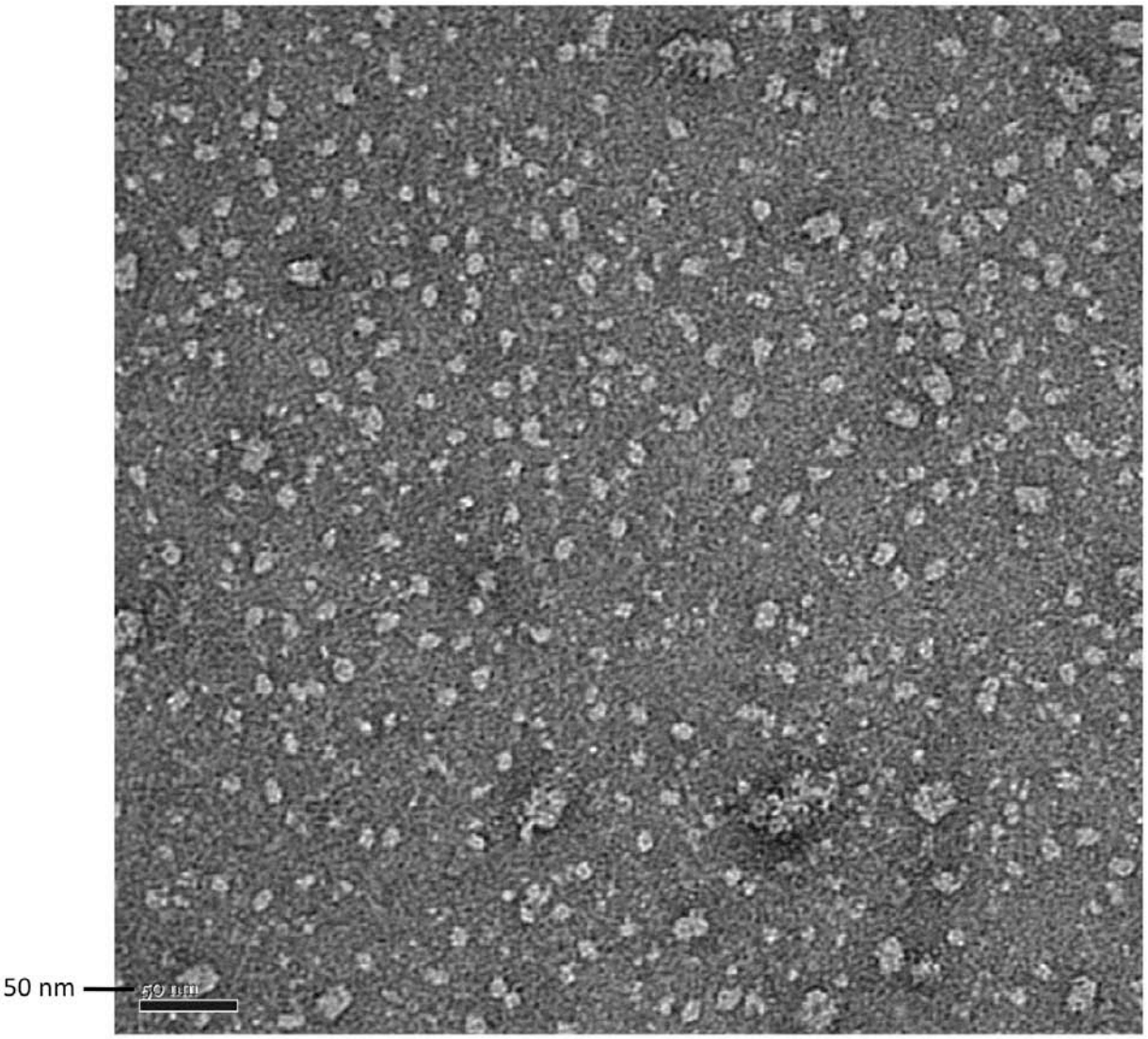

Supplementary Figure 3. Negative stain EM image of the UCP2 NMR sample. Images recorded at 120 kV on a FEI Tecnai T12 electron microscope equipped with a 4k x 4k Gatan CCD camera.

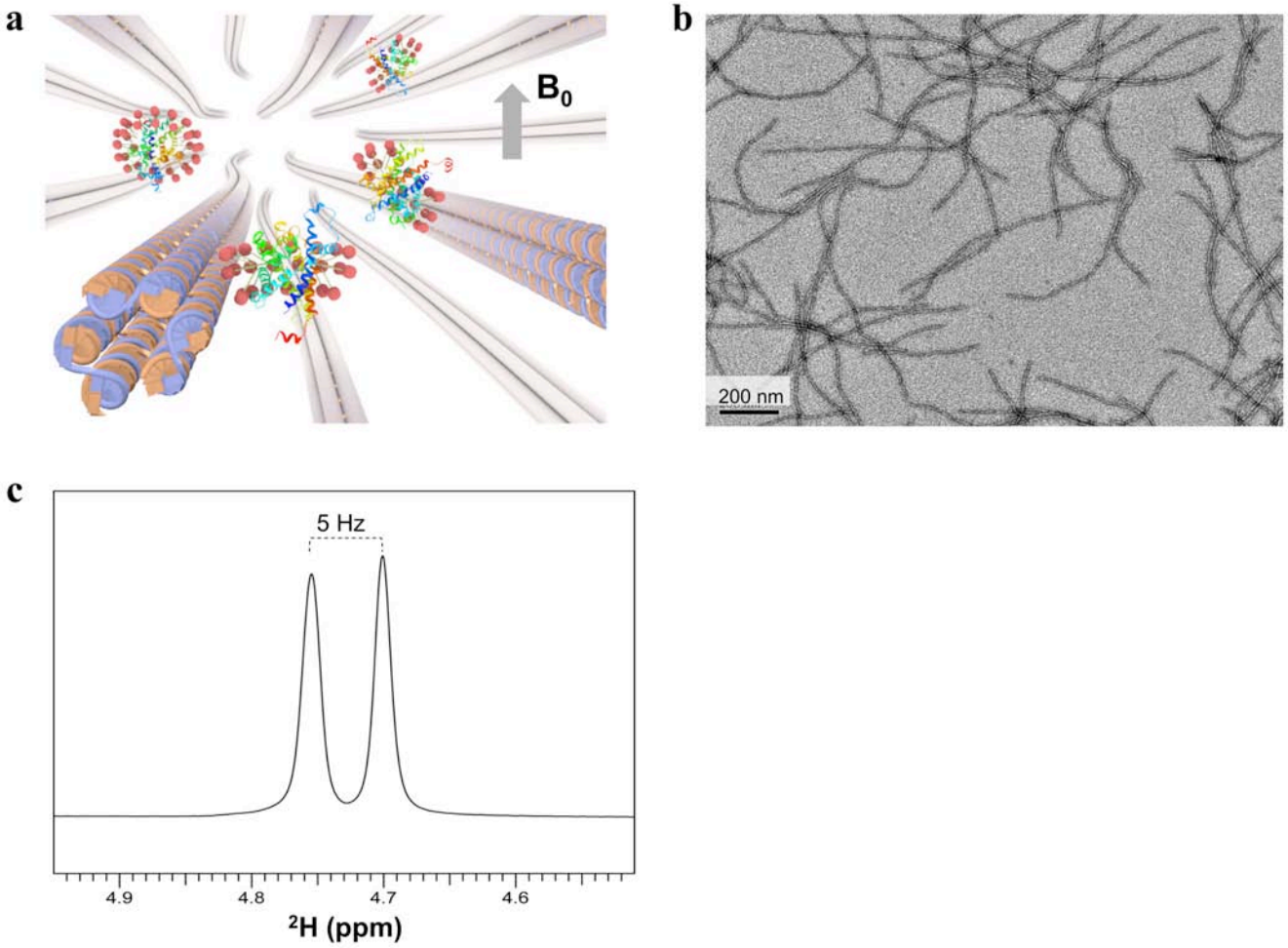

Supplementary Figure 4. Characterization of DNA nanotubes. **a,** Cartoon drawing shows the utility of DNA nanotube liquid crystal to achieve marginal alignment of UCP2-detergent complex in the static magnetic field. **b,** Negative-staining EM image of the nanotubes prepared as described above in Supplementary Methods. **c,** ^{2}H quadrupolar splitting of D_2O in the aligned sample containing 0.5 mM UCP2 and 20 mg/ml DNA nanotubes (all other buffer components same as those in the NMR sample described in METHODS). The 1D spectrum was recorded at ^{1}H frequency of 600 MHz.

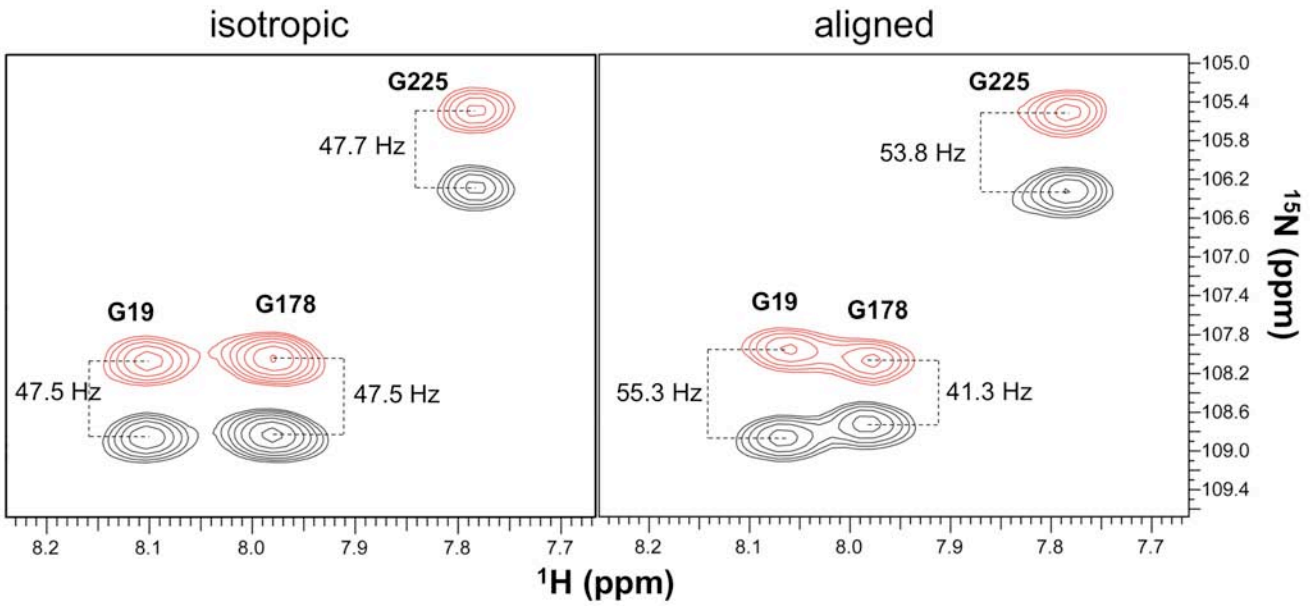

Supplementary Figure 5. Measurement of RDCs of UCP2 weakly aligned in the DNA nanotube liquid crystal. The example shows regions of the *J*-scaled TROSY-HNCO spectra recorded with an isotropic sample (left) and an aligned sample (right) at ^{1}H frequency of 600 MHz. For both isotropic and aligned samples, two inter-leaved spectra were recorded, the regular TROSY-HNCO (black peaks) and also a modified TROSY-HNCO with J_{NH} evolution during the ^{15}N chemical shift evolution scaled to zero (red peaks). The difference in 15N frequency between the red and black peaks is either $^{1}J_{NH}/2$ for the isotropic sample or $(^{1}J_{NH}+^{1}D_{NH})/2$ for the aligned sample. $^{1}D_{NH}$ can be determined from the two values.

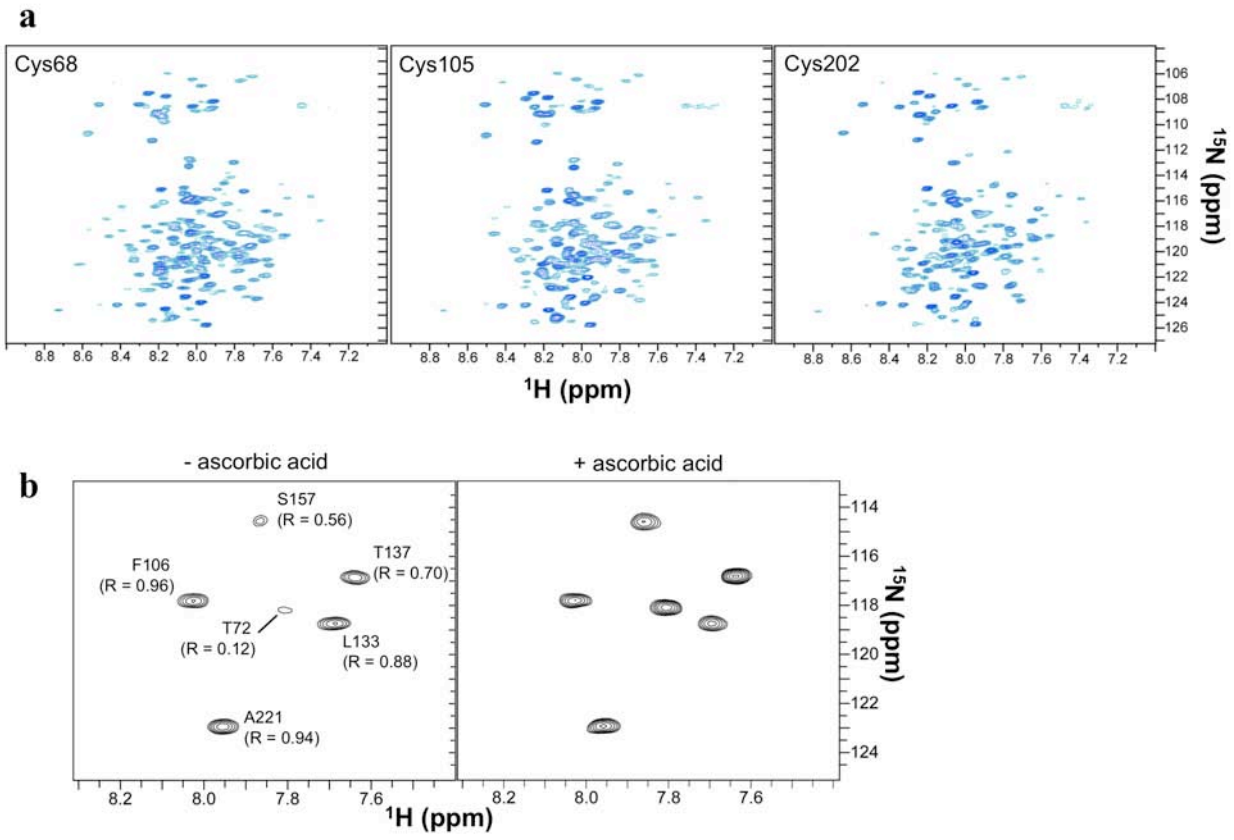

Supplementary Figure 6. PRE measurements in spin-labeled UCP2. a, ^{1}H-^{15}N TROSY-HSQC spectra of 3 UCP2 samples with single nitroxide labeled at different cysteine positions. The spectra were recorded after the nitroxide was reduced by the ascorbic acid. **b,** Residue-specific broadening of NMR resonance by a particular spin label (in this case at position 68) was measured with two 3D TROSY-HNCO spectra, one recorded after nitroxide labeling (left) and another after reducing the nitroxide free electron with a 5x molar ascorbic acid (right).

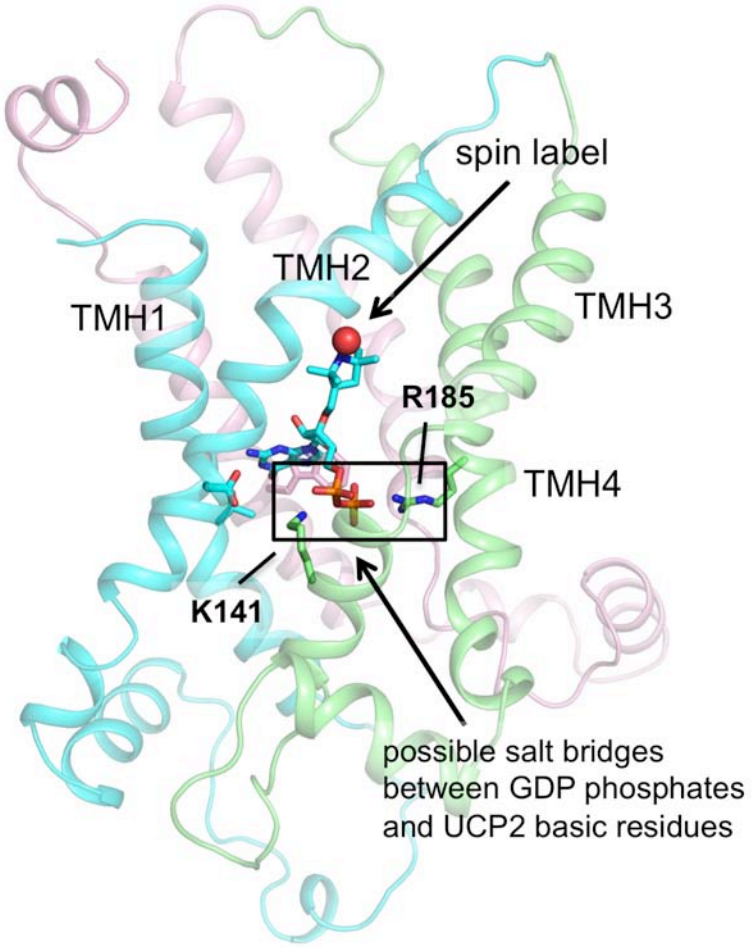

Supplementary Figure 7. Speculative model of nitroxide-labeled GDP (NO-GDP) binding to UCP2. The position of the nitroxide radical (red sphere) is roughly given by the semi-quantitative PRE restraints. We then placed the GDP portion of the NO-GDP by maximizing electrostatic interactions between GDP and charged residues in the channel, including the plausible salt bridges between the GDP phosphates and Lys141 and Arg185. The depth of NO-GDP in the UCP2 channel is similar to that of the proposed binding of ADP in the ANT1 channel[4,5].

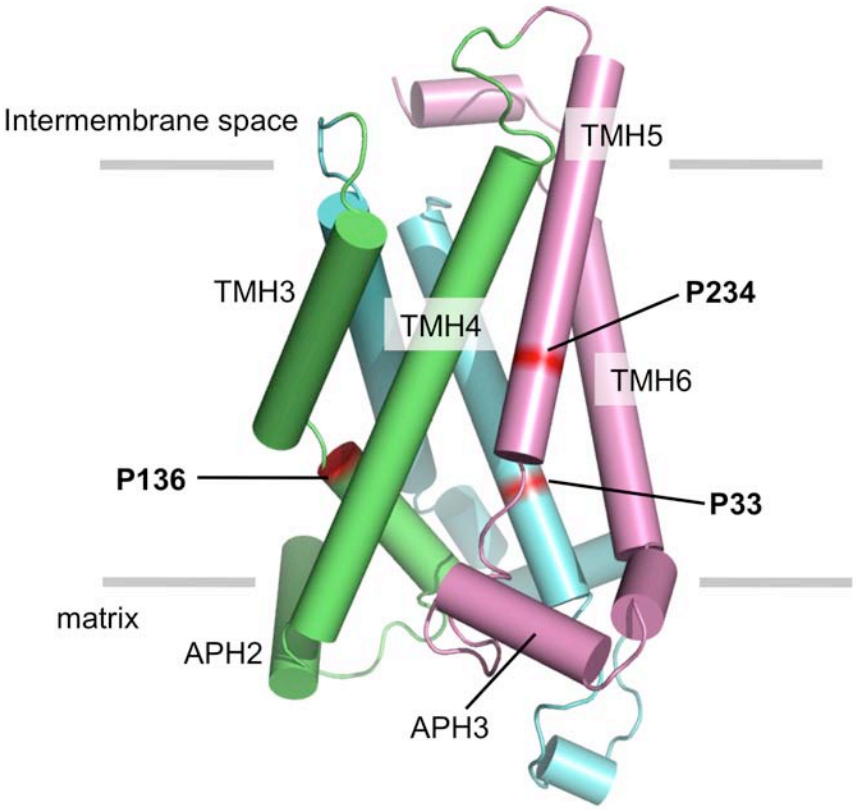

Supplementary Figure 8. Conformational deviation of repeat 3 from that of the other two repeats in GDP-bound UCP2. The side view (or viewing from the membrane side) reveals that TMH5 of repeat 3 is farther away from the matrix side compared to TMH1 and TMH3 of repeats 1 and 2, respectively. Positions of the 3 conserved prolines at the proline kinks of TMH 1, 2, and 3 (P33, P136, P234; numbered as in **Fig. 3a**) are a good indicator of breaking of the 3-fold pseudo-symmetry by repeat 3. When aligning the sequences of the 3 repeats, P33, P136 and P234 are aligned and this property is highly conserved in other carriers. This cartoon view shows that P234 is significantly closer to the intermembrane side of the carrier protein compared to P33 and P136.

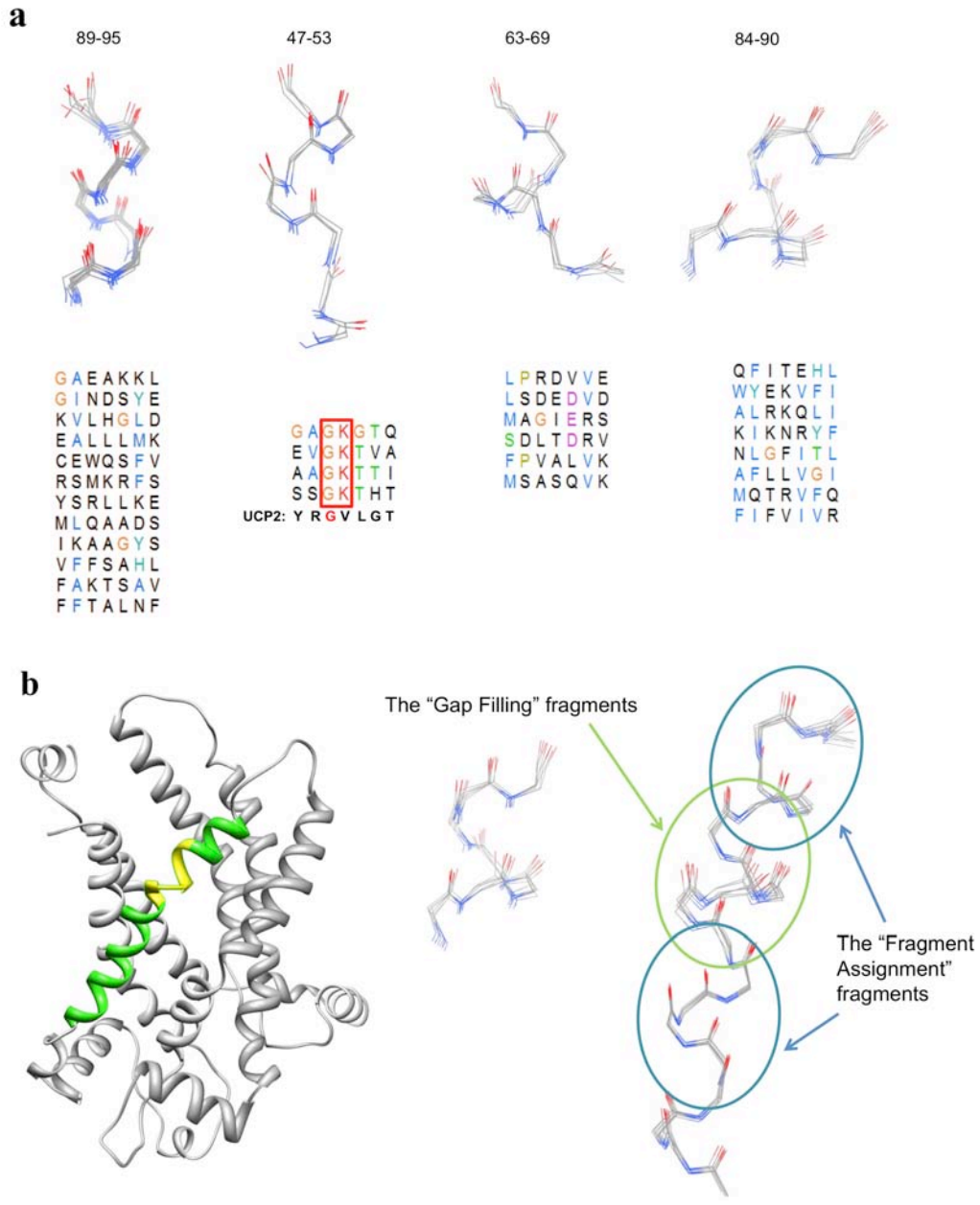

Supplementary Figure 9. Examples of fragment convergence. **a,** Four representative fragment classes matching our RDC data with Q_{free} < 25%. Fragments were super-imposed to minimize r.m.s. deviations. The amino acid sequences of the fragments are shown below each fragment ensemble. In most cases, our RDC data match backbone conformations in a sequence-independent manner. However, for residues 47-53, the glycine position is conserved in all fragments with good Q_{free} scores. **b,** An example of using gap filling fragments (yellow, in the ribbon structure on the left) to bridge two fragments of TMH2 shown in green. Each member of the gap filling fragment ensemble (middle) was inserted, generating a bundle of the merged segments with low r.m.s. deviation (right). The six merged segments all have Q_{free} < 0.25.